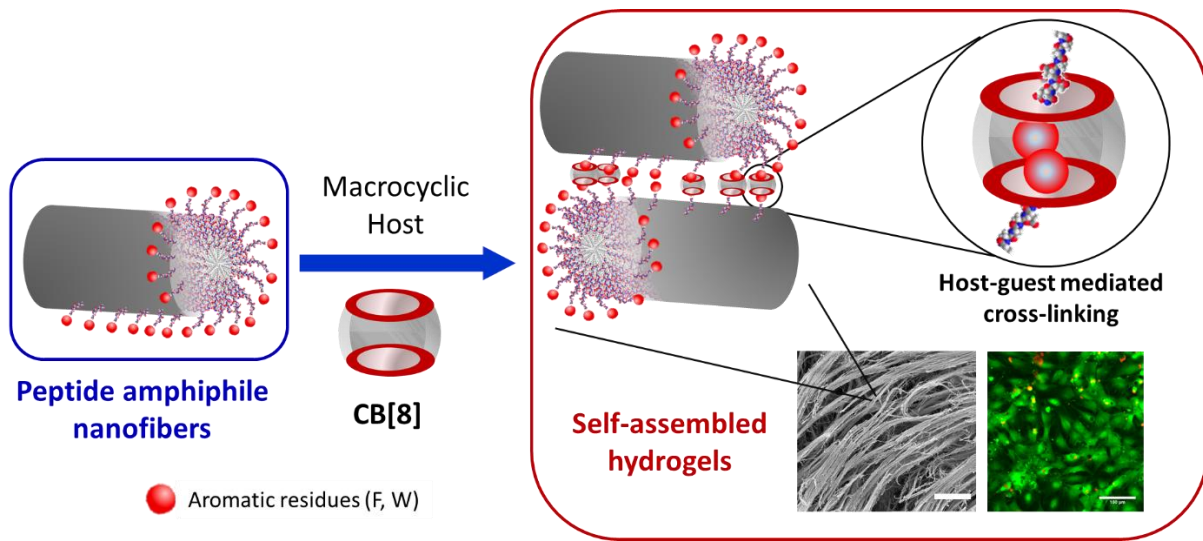


TOC graphical abstract



Peptide amphiphile hydrogels based on homoternary cucurbit[8]uril host-guest complexes

Carlos Redondo-Gómez^{a,b,c}, Soraya Padilla-Lopátegui^{a,b}, Alvaro Mata^{a,b,d,e,f}, Helena S. Azevedo^{a,b}**

^a School of Engineering & Materials Science, Queen Mary University of London, London E1 4NS, UK

^b Institute of Bioengineering, Queen Mary University of London, London E1 4NS, UK

^c National Nanotechnology Laboratory LANOTEC, National Center for High Technology CeNAT, 1174-1200 Pavas, San José, Costa Rica

^d School of Pharmacy, University of Nottingham, University Park, Nottingham NG7 2RD, UK

^e Department of Chemical and Environmental Engineering, University of Nottingham, University Park, Nottingham NG7 2RD, UK

^f Biodiscovery Institute, University of Nottingham, University Park, NG7 2RD, UK

*Corresponding authors:

Helena Azevedo

h.azevedo@qmul.ac.uk

Alvaro Mata

a.mata@nottingham.ac.uk

ABSTRACT

Supramolecular hydrogels based on peptide amphiphiles (PAs) are promising materials for tissue engineering and model extracellular matrixes for biological studies. While PA hydrogels are conventionally formed via electrostatic screening, new hydrogelation mechanisms might help to improve the design and functionality of these materials. Here, we present a host-guest-mediated PA hydrogelation method that relies on the formation of a host-guest homoternary complex with cucurbit[8]uril (**CB[8]**) and aromatic amino acid-bearing PA nanofibers. As a result of the host-guest crosslinking between PA nanofibers, hierarchical morphologies and increased stiffness were found when host-guest mediated PA hydrogels were compared to their ion-based equivalents. Additionally, both families of hydrogels exhibited similar biocompatibilities. These results demonstrate that **CB[8]**-mediated hydrogelation can be used as an alternative crosslinking method to upgrade the design of PA materials and extend their biomedical applications.

KEYWORDS: Host-guest, peptide amphiphile, hydrogel, aromatic interactions, supramolecular, biomaterials.

INTRODUCTION

Supramolecular chemistry enables the design of materials through noncovalent forces while guiding biomolecular self-organization and recognition.^{1,2} This capability has inspired the generation of self-assembling materials based on polymers,^{3,4} sugars,⁵ nucleic acids,⁶ proteins,^{7,8} peptides^{9,10}, and their combination¹¹ exhibiting tuneable, dynamic, and modular control over morphological and functional properties. In particular, peptide-based supramolecular hydrogels have facilitated the use of nature inspired motifs and non-covalent interactions to engineer bioactive hydrogels comprising well-defined nanostructures.¹²

Peptide amphiphiles (PAs) are a comprehensively studied family of self-assembling peptides programmed to form fibrillar 1D structures in aqueous environments.¹³ PA molecules comprise a lipid hydrophobic tail, a β -sheet forming segment, and a polar head of amino acid residues often designed to carry biofunctional epitopes. Either pH changes or the presence of counter ions produce charge screening of these segments, triggering self-assembly and the formation of nanofibrous 3D hydrogels that mimic the natural extracellular matrix (ECM).¹⁴ These hydrogels have proved their versatility and broad utility serving as bioactive matrixes capable of promoting specific cell behaviours such as migration¹⁵ and differentiation¹⁶; *in vivo* regeneration of tissues such as neurons,¹⁷ blood vessels,¹⁸ bone,¹⁹ and cartilage;²⁰ and recreating complex *in vivo* environments *in vitro* such as bone-like constructs²¹ or tumour microenvironments.²²

Host-guest interaction motifs have increasingly been used in the design of supramolecular materials by enabling formation of complexes between a suitable macrocycle (most commonly a cyclodextrin or a cucurbit[n]uril) with appended guests on polymer chains.²³ This approach has been primarily employed in the design of polymer-based hydrogels, bestowing these materials with self-healing or adaptable crosslinks suitable for modulating the crosslinking density without changing the network connectivity of the hydrogel.^{24,25} We have previously reported on the incorporation of host-guest adamantane/ β -cyclodextrin functionalities within PA molecules as molecular cues to enhance mechanical properties²⁶ and epitope presentation²⁷ of PA hydrogels. Furthermore, Stupp and co-

workers have also recently reported on superstructure formation resulting from molecular exchange of β -cyclodextrin and adamantane functionalized PAs, which lead to morphological and rheological changes in the resulting hydrogels.²⁸ These studies demonstrate the opportunities that host-guest approaches could offer to enhance control, modularity, hierarchy, and functionality of peptide-based supramolecular hydrogels.

Cucurbit[8]uril (**CB[8]**) is a macrocyclic octamer of glycoluril units bound together by 16 methylene bridges (Scheme 1).^{29,30} **CB[8]** features two identical polar portals to a hydrophobic cavity that is large enough to simultaneously accommodate two small organic aromatic guests.³¹ This structure enables the formation of highly stable ternary complexes with a variety of small chemical species,^{32,33} such as aromatic amino acids, including tyrosine (Y),³⁴ phenylalanine (F), and tryptophan (W). The amino acids F and W have been reported to selectively bind to **CB[8]** forming a 2:1 homoternary complex in several systems, including tri-³⁵ and oligopeptides,³⁶ and macromolecular systems including proteins,³⁷ enzymes,³⁸ polysaccharide derivatives,³⁹ intracellular drug delivery systems,⁴⁰ polymer nanoparticles,⁴¹ and styrenic polymer-based hydrogels.⁴²

In this work, we introduce a new class of host-guest PA molecules (Scheme 1) able to undergo conventional ion-mediated gelation and form supramolecular hydrogels via homoternary host-guest complexes with **CB[8]**. We describe the synthesis and provide host-guest complexation mechanism, thorough spectroscopic characterisation, as well as assessment of the mechanical properties of the resulting hydrogels, and their suitability to be used as tuneable matrixes for cell culture.

EXPERIMENTAL SECTION

Materials

Cucurbit[8]uril (**CB[8]** hydrate, 99+%) was purchased from abcr GmbH (Karlsruhe, Germany). Phosphate buffered saline (PBS 1x), 4-(2-hydroxyethyl)piperazine-1-ethanesulfonic acid (HEPES), Dulbecco's Modified Eagle's Medium (DMEM), Hank's Balanced Salt Solution (HBSS), Penicillin/Streptomycin (P/S), and Foetal Bovine Serum (FBS), were obtained from Gibco (Life Technologies). All other reagents were purchased from Sigma-Aldrich and used without any further purification unless otherwise stated.

Methods

Peptide synthesis and purification. Peptide amphiphiles (PAs) **E₃-PA**, **G₅F-PA** and **G₅W-PA** (Scheme 1) were synthesised using modifications of previously reported solid phase peptide synthesis (SPPS) procedures.⁴³ PAs were purified using reverse phase HPLC (RP-HPLC) using a 2545 Binary Gradient Preparative HPLC (Waters, USA) and a C18 column (Atlantis Prep OBD T3 Column, Waters, USA). Peptide identity was confirmed using electrospray ionisation mass spectrometry (ESI-MS, Thermo LXQ, Thermo Scientific, USA). Further synthesis and characterisation details are provided in the Electronic Supporting Information.

Nuclear magnetic resonance (NMR). PAs were dissolved in D₂O at a final concentration of 4-6 mg/mL (ammonium-d₄ deuterioxide, ND₄OD, was added to promote peptide solubility) and 1 equivalent of **CB[8]** in D₂O was added to the mixture. Spectra were acquired using a Bruker AvanceNEO 600 spectrometer at room temperature.

Fluorescence spectroscopy. Fluorescence spectra were recorded on a LS55 spectrofluorimeter with Xenon pulsed flash lamp (Perkin Elmer, MA, USA). Measurements were made using a 10 mm path-length cuvette at 25 °C and a λ_{exc} = 280 nm. Emission spectra were recorded from 300 nm to 600 nm in each case.

Circular dichroism (CD). CD measurements were made using a 1 mm path-length quartz cuvette placed in a Pistar-180 spectropolarimeter (Applied Photophysics, Surrey, UK) equipped with a Peltier temperature controller, under a continuous nitrogen purging at a constant pressure of 0.7 MPa and temperature of 25 °C. PAs were dissolved in 10 mM HEPES saline (155 mM NaCl) buffer (pH 7.4) reaching a final concentration of 0.01 wt% ($[\mathbf{E}_3\text{-PA}] = 87 \mu\text{M}$, $[\mathbf{G}_5\mathbf{F}\text{-PA}] = 63 \mu\text{M}$, $[\mathbf{G}_5\mathbf{W}\text{-PA}] = 62 \mu\text{M}$). Far UV spectra were recorded from 190 to 260 nm at wavelength step of 0.5 nm. Each represented spectrum is the average of three consecutive spectra. Temperature variable CD experiments were carried out between 10 °C and 70 °C, with a heating rate of 1 °C/min.

Transmission Electron Microscopy (TEM). PA solutions (0.05 wt% in HEPES buffer, $[\mathbf{E}_3\text{-PA}] = 0.435 \text{ mM}$, $[\mathbf{G}_5\mathbf{F}\text{-PA}] = 0.315 \text{ mM}$, $[\mathbf{G}_5\mathbf{W}\text{-PA}] = 0.310 \text{ mM}$) were negatively stained as follows: solutions were drop-casted on holey carbon-coated copper TEM grids (Agar Scientific, Stansted, UK), solution excess was blotted after 5 min incubation, followed by one minute incubation with 2% uranyl acetate. Grids were then washed with ultrapure water for 30 s and air dried for 24 h at room temperature before imaging. Bright-field TEM images were acquired on a JEOL 1230 Transmission Electron Microscope operated at 80 kV. All the images were recorded by a Morada CCD camera (Image Systems) and at least six areas were analysed (corresponding to $n \geq 100$ PA fibers).

Gel preparation. In a typical example of hydrogelation procedure, PAs were dissolved in HEPES saline buffer at a concentration of 1.5 wt%, incubated at 80 °C for 30 min and let slowly cool down to 25 °C (“peptide stock solution”). Subsequently, a 30 μL drop of peptide stock solution was placed onto a poly-dimethylsiloxane (PDMS) support, injected with 15 μL of either 100 mM CaCl_2 or 350 μM saturated **CB[8]** solution and incubated at 28 °C for 24 h to afford 1 wt% hydrogels in all cases.

Scanning Electron Microscopy (SEM). PA hydrogel samples underwent stepwise dehydration, critical point drying and gold coating before SEM imaging. Initially PA hydrogels were stepwise dehydrated by immersion in increasingly concentrated ethanol solution (20%, 50%, 70%, 80%, 90%, 95%, 100%), for 5 min twice in each solution. Dehydrated samples were dried using a critical point dryer

(K850, Quorum Technologies, UK) and gold coated before imaging on an Inspect F50 (FEI Company, the Netherlands) ($n \geq 3$).

Oscillating rheology. Rheological characterisation was performed with a DHR-3 Rheometer (TA Instruments, USA) using an 8 mm diameter parallel plates geometry. G' (storage modulus) and G'' (loss modulus) of hydrogels were monitored by amplitude and frequency sweeps. G' and G'' moduli were measured at 25 °C and a constant frequency of 1 Hz in the 0.01% – 10% strain during the amplitude sweep, while the oscillation frequency experiments were carried out at a 0.1% fixed strain along a 0.1 – 100 Hz range.

Cell culture experiments

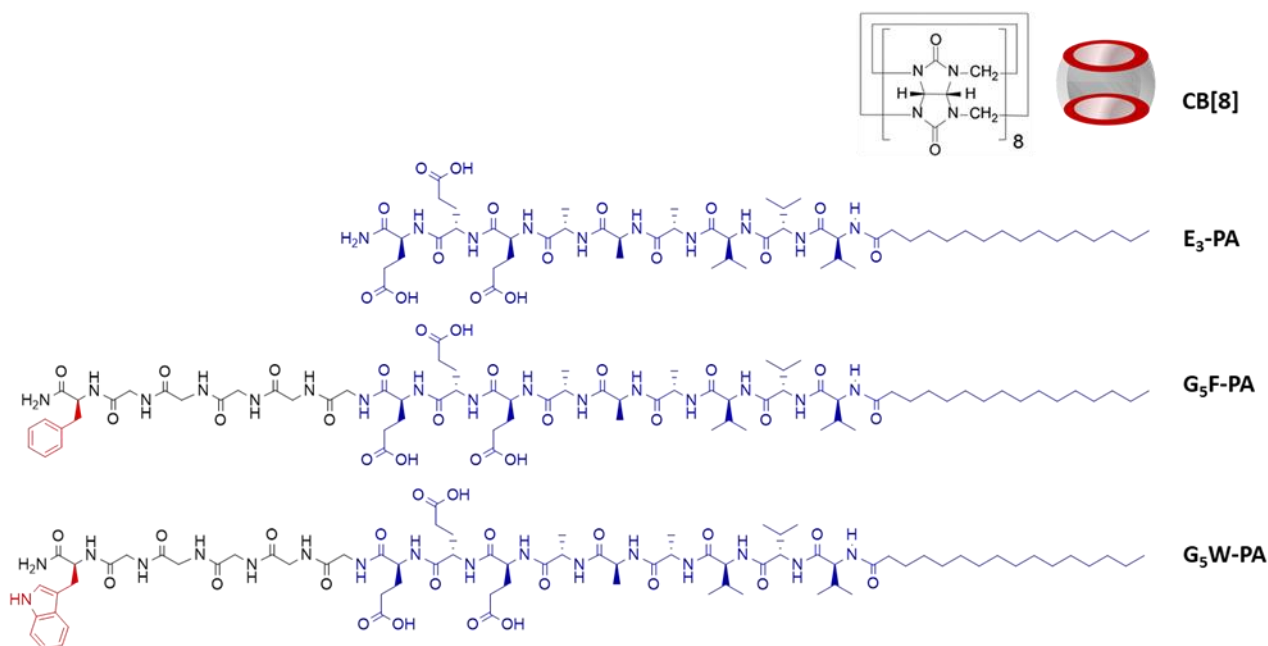
All cell culture experiments were conducted using NIH-3T3 fibroblasts. NIH-3T3 fibroblasts were cultured with DMEM medium supplemented with 10% fetal bovine serum (FBS) and 1% penicillin and 1% streptomycin. Cells were maintained in a humidified 5% CO₂ atmosphere at 37 °C during culture.

In vitro cell viability assays atop hydrogels. Hydrogels were sterilised using UV light for 30 min prior to culture. Typically, 30000 NIH-3T3 fibroblasts were seeded on top of a hydrogel, placed under orbital agitation for 1 h and then incubated for 24 h until LIVE/DEAD imaging. A LIVE/DEAD Viability/Cytotoxicity Assay Kit (Thermo Fisher Scientific, UK) was used. Cells were incubated in 10 mM calcein AM and 1 mM ethidium homodimer-1 (EthD-1) dissolved in DMEM for 30 min before imaging, stained samples were visualised on an inverted epifluorescence widefield Leica DMI4000B microscope (Leica, Germany) equipped with a LEICA DFC300 FX CCD camera.

RESULTS AND DISCUSSION

Design and rationale of guest-PA molecules

We designed two anionic guest-PA molecules isostructural to **E₃-PA** (C₁₆-V₃A₃E₃), whose supramolecular aggregation has been reported.¹⁵ Both guest-PAs bear aromatic amino acids (phenylalanine F and tryptophan W) known to form complexes with **CB[8]**.^{35,42} Furthermore, both guest-PAs (sequence: C₁₆-V₃A₃E₃G₅X) comprise an aliphatic palmitoyl tail (C₁₆-) at their N-terminus, a β -sheet forming amino acid sequence (V₃A₃), and three ionisable glutamic acid residues (E₃) to promote nanofiber solubility in water. In order to promote display of the aromatic amino acid residues (X), a pentaglycine (G₅) spacer was included to provide a ~ 19.3 Å space from the negatively charged fiber region.⁴⁴ This combination of structural features allows for surface display of either a phenylalanine (X = F in **G₅F-PA**) or a tryptophan (X = W in **G₅W-PA**) residue once the PA monomers self-assemble into nanofiber (Scheme 1). Control **E₃-PA** and guest-PAs (**G₅F-PA** and **G₅W-PA**) were synthesized using standard solid-state peptide synthesis (SSPS) followed by purification through reverse phase High-Performance Liquid Chromatography (RP-HPLC) as previously described (Figure S1-3, Table S1).⁴³



Scheme 1. Molecular structures of CB[8] and peptide amphiphile (PA) molecules used in this study. All PA molecules are isostructural to the negatively charged **E₃-PA**. Five glycine residues were included as spacer, followed by either a phenylalanine or a tryptophan residue in **G₅F-PA** and **G₅W-PA** respectively.

Guest-PA supramolecular self-assembly in solution

We initially investigated the possibility of presenting G₅F and G₅W motifs at the surface of self-assembled PA nanofibers. **G₅F-PA** and **G₅W-PA** nanofiber self-assembly was investigated using transmission electron microscopy (TEM). TEM micrographs evidence the presence of micron-long nanofibers of around 11-14 nm diameter from both guest-PA solutions at 25 °C. **G₅F-PA** generated stand-alone nanofibers (Figure 1A), whereas **G₅W-PA** nanofibers appear to coalesce into submicron-size bundles (Figure 1C). A more robust stacking between adjacent indole rings of tryptophan residues in **G₅W-PA** can account for this tendency to form bundles, which was not observed in **G₅F-PA** under the same micromolar concentration regime. The presence of aggregate structures seen in the TEM images of both guest-PAs, from relatively diluted solutions, indicates working conditions above their critical aggregation concentration, which typically falls in the micromolar concentration regime, even for tryptophan-bearing PA molecules of comparable length to **G₅F-PA** and **G₅W-PA**.^{45,46}

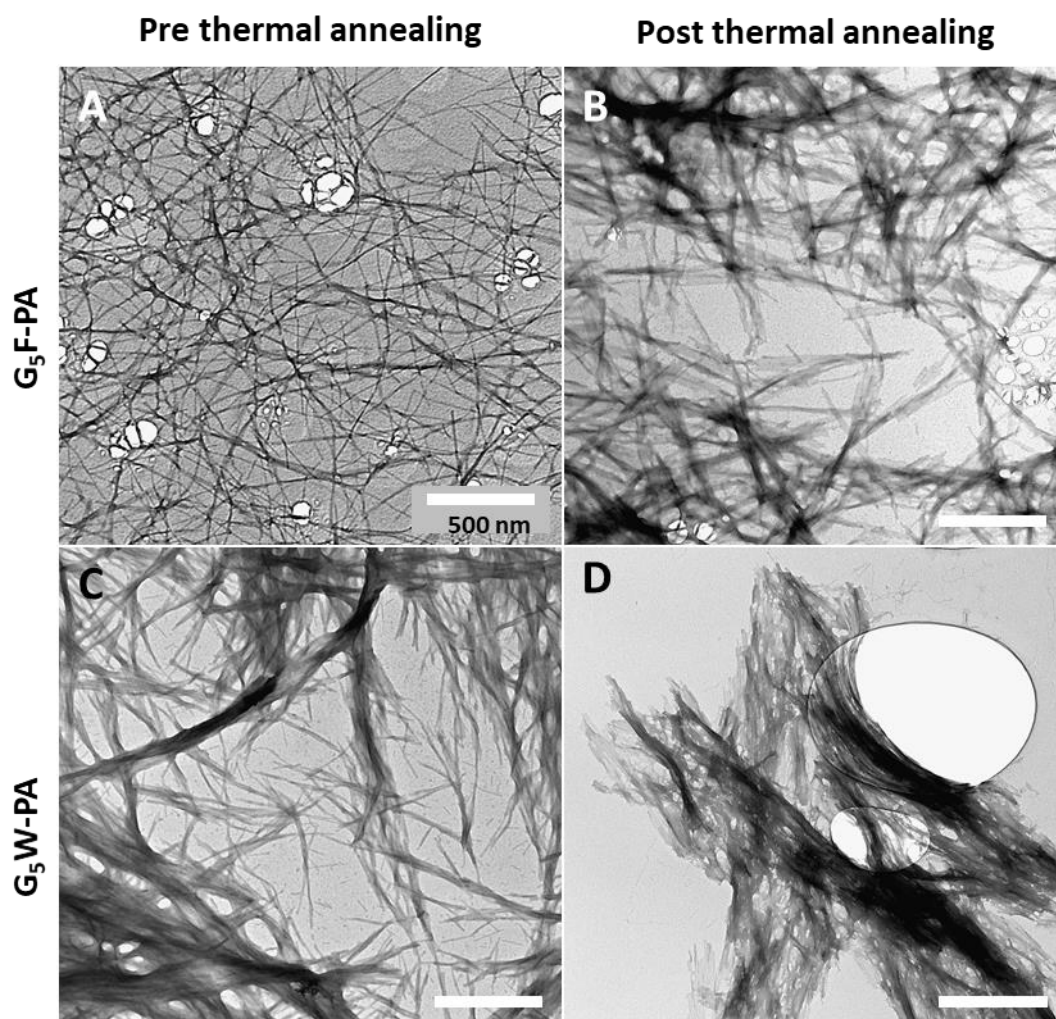


Figure 1. Self-assembly of **G₅F-PA** and **G₅W-PA** into nanofibers. (A) TEM micrographs of **G₅F-PA** and (C) **G₅W-PA** at 25 °C. (B, D) TEM micrographs of the same PA solutions thermally treated at 80 °C ($[\text{G}_5\text{F-PA}] = [\text{G}_5\text{W-PA}] = 63 \mu\text{M}$, in HEPES buffer).

Negatively charged PA molecules analogue to **E₃-PA** (therefore, analogue to **G₅F-PA** and **G₅W-PA** as well) offer the possibility to access hierarchical nanofiber ordering levels via a thermal process (as detailed in the Experimental Section). Such process renders long-axis nanofibers out of a randomly ordered fiber array in solution,⁴⁷ and this process is known to externally expose the amino acid cap and to aggregate internally the palmitoyl tail by an entropy driven dehydration-rehydration process.¹⁵ In order to explore the possibility of nanofiber alignment in our guest-PAs **G₅F-PA** and **G₅W-PA**, PA solutions were heated at 80 °C and then slowly cooled down to room temperature. In the case of **G₅F-PA**, TEM micrographs revealed the formation of intertwined filaments with larger diameters

after thermal annealing (Figure 1B) than the pristine nanofibers (Figure 1A), while **G₅W-PA** bundles turned into micron-sized aggregates with highly parallel oriented filaments (Figure 1D). These large bundles are likely to arise as a result of hydrophobic and aromatic interactions among tryptophan residues located in the periphery of the fibers. These results demonstrate that the presence of G₅F or G₅W motifs at the surface of PA nanofibers neither disrupts fiber formation nor interferes with their nano- to microscale hierarchical self-assembly via thermal annealing.

Guest-PA-CB[8] host-guest interactions

Homoternary complex formation

As PA nanofibers with pendant phenylalanine and tryptophan amino acids were found to assemble in solution, we hypothesised that these aromatic residues might form their corresponding inclusion complex with **CB[8]**. ¹H-NMR spectroscopy revealed changes in the chemical shifts of the signals between 7.1 and 7.8 ppm, corresponding to the protons of the phenyl and indole ring in **G₅F-PA** and **G₅W-PA**, respectively. This finding suggests the placement of these residues in a new magnetic environment when in presence of **CB[8]** (Figure S4 & Figure S5). Monitoring fluorescence of aromatic motifs through the method of continuous variations⁴⁸ (Figure S6) allowed to obtain the corresponding Job Plots shown in Figure 2A, whose maxima around 0.66 PA mole fraction confirms the expected 2:1 binding mode and the formation of the homoternary complexes (**G₅F-PA**)₂⊂**CB[8]** and (**G₅W-PA**)₂⊂**CB[8]**. The slightly steeper triangular-like shape originated by **G₅F-PA** might be an indicator of a greater affinity towards **CB[8]** than **G₅W-PA**.⁴⁸ Affinity constant values (ternary K_{eq}) have been determined to be around 10⁹-10¹² M⁻² for similar **CB[8]**-Phe and **CB[8]**-Trp complexations.^{35,42} However, careful consideration should be taken to estimate these values in self-assembling systems such as PA-nanofibers, as **CB[8]**-guest interactions are well-known to be sensitive to a number of variables. For example, restrictions imposed by the self-assembly of PA monomers into nanofibers might have an effect on rotational and conformational availability of Phe and Trp residues. In addition, **CB[8]** is also known to be highly selective, not only for these residues,

but also for their placement in the peptide sequences as a function of their distance from the C-terminus end.³⁵

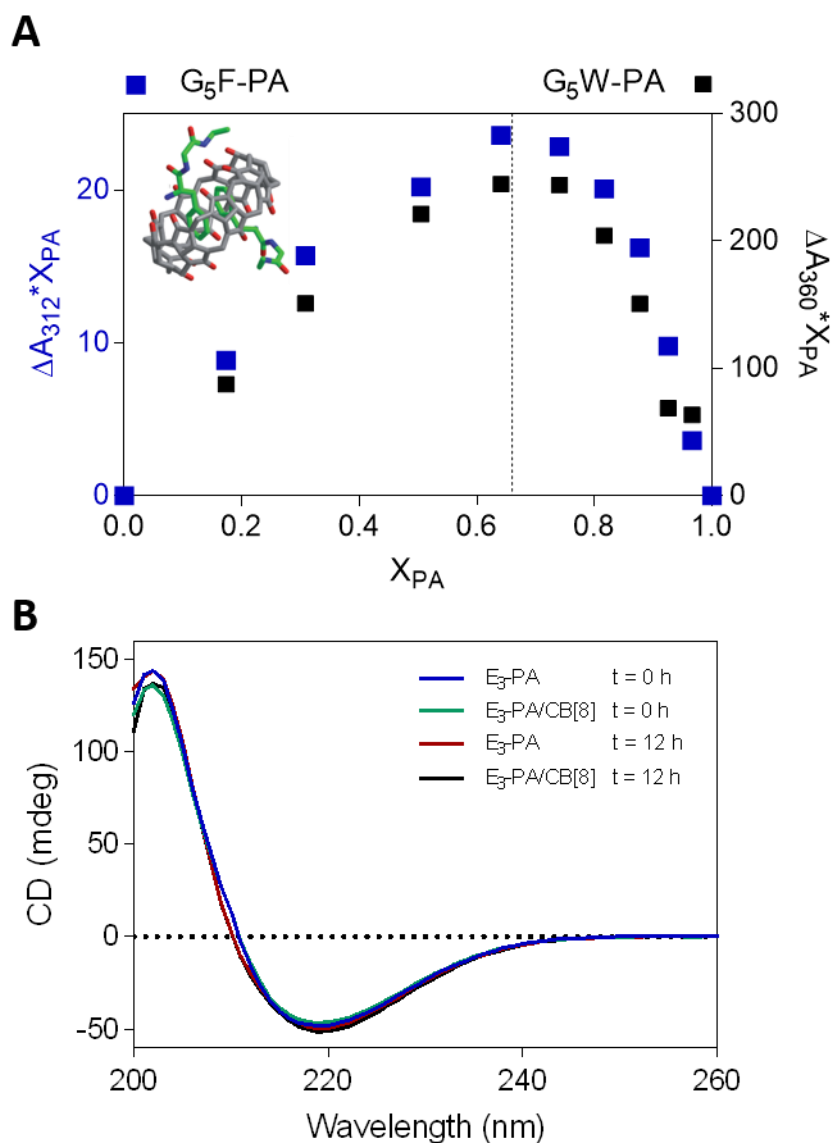


Figure 2. Host-guest interaction between PAs and their complementary macrocyclic host **CB[8]** in aqueous media. A) Fluorescence spectroscopy revealed the formation of $(G_5F-PA)_2 \subset CB[8]$ and $(G_5W-PA)_2 \subset CB[8]$ 2:1 complexes. B) Circular dichroism (CD) shows no evidence of intermolecular binding between control **E₃-PA** and **CB[8]**.

Inclusion of PA molecules can be accounted by three main driving forces: the release of ‘high-energy’ water molecules upon complexation, the formation of hydrogen bonds between the N-H protons from peptide bonds in PAs and N-H protons from both of **CB[8]** carbonyl portals,³² and the formation of

intermolecular aromatic interactions between aromatic motifs from PAs. In fact, aromatic interactions seem to play a key role, as **CB[8]** appears not to interact with PA molecules lacking the G₅F or G₅W motifs, as revealed by circular dichroism (CD) on **E₃-PA/CB[8]** (Figure 2B). These results demonstrate that PA molecules can take part in homoternary host-guest complexations with a suitable macrocyclic host.

Host-guest interactions affect nanofiber conformation

As formation of **(G₅F-PA)₂⊂CB[8]** and **(G₅W-PA)₂⊂CB[8]** complexes were evidenced, we decided to investigate possible effects on the secondary structure of the self-assembled nanofibers. CD investigations showed that both **G₅F-PA** and **G₅W-PA** nanofibers exhibit a β -sheet signature signal, characterised by a positive maximum centred at 205 and 203 nm, respectively (Figure 3A,D), whereas in presence of **CB[8]** both CD signals experience an apparent red-shift and a significant increase in intensity. A similar red-shift was observed in the negative minima centered around 220 and 218 nm. These red-shifts can be attributed to increasing levels of twisting of β -sheets at the nanofibers core (as proposed by Edelbrock et al. in an anionic host-guest-based system)²⁸ while the intensity increase can be the result of re-arrangement of these β -sheets into longer and more regular ones as a result of the binding with **CB[8]**.⁴⁹

In the case of **G₅W-PA/CB[8]** mixtures, an intensity increase in the positive maximum centered at 203 nm is observed. This change is consistent with the twisting of β -sheets in nanofibers, even though **CB[8]** gave rise to the appearance of a positive maximum at 231 nm (Figure 3D) inconsistent with this secondary structure. Trp residues have been reported to contribute positively to this region of CD spectra when part of β -strands, especially in proteins containing several Trp moieties.⁵⁰ In the case of **G₅W-PA/CB[8]** this positive band can be attributed to close intermolecular contacts between indole rings from adjacent Trp residues,^{51,52} as in the case of PEG-ylated Trp-containing amphiphiles,⁵³ or Trp-bearing polymers where indole sidechain groups get located in dissymmetric environments.⁵⁴

CD investigations demonstrated how the formation of homoternary $(\text{PA})_2\text{CB}[8]$ complexes is temperature sensitive, maintaining significant degrees of interaction at physiologically relevant temperatures, and disassembling above 60 °C (Figure 3B,E). We also investigated the effect of incubating $\text{PA}/\text{CB}[8]$ solutions at 25 °C for 12 h, finding that $(\text{PA})_2\text{CB}[8]$ complexes exhibited conformational changes. The negative minimum, originally centered at 223 nm in $(\text{G}_5\text{F-PA})_2\text{CB}[8]$ nanofibers, exhibited a 3 nm red-shift, indicating further β -sheet twisting after initial fiber preparation (Fig 3C), while the $(\text{G}_5\text{W-PA})_2\text{CB}[8]$ positive maximum lost about 25% of its initial intensity, indicating a possible loss of β -sheet length and regularity due to ageing (Figure 3F). These results demonstrate that supramolecular complexations at the periphery of guest-PA nanofibers can lead to conformational changes in peptide monomer units. These findings are in good agreement with other host-guest PA systems based on adamantane/ β -cyclodextrin interactions.²⁶

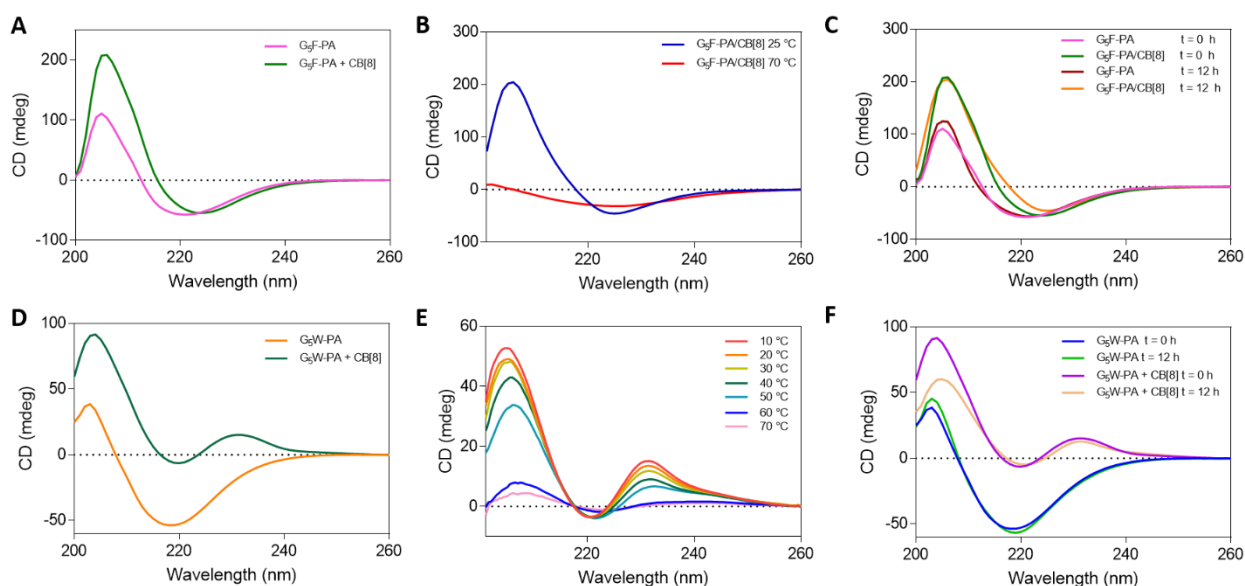


Figure 3. Guest-PA secondary structures in presence of **CB[8]** in aqueous media. A) CD spectra of **G₅F-PA** and its **CB[8]** mixture exhibit β -sheet conformations. B) Temperature variable CD shows how these β -sheets are temperature sensitive. C) Time evolution of **G₅F-PA** self-assembled nanofibers and the ternary complex $(\text{G}_5\text{F-PA})_2\text{CB}[8]$. D) **G₅W-PA** nanofibers exhibit β -sheet conformation, while interaction with **CB[8]** produces radical changes in its CD spectra. E) CD studies indicate that $(\text{G}_5\text{W-PA})_2\text{CB}[8]$ formation is temperature sensitive. F) **G₅W-PA** shows little time-evolution in its secondary structure, while the ternary complex $\text{CB}[8]\cdot(\text{G}_5\text{W-PA})_2$ exhibits loss of β -sheet content after 12 h of incubation at 25 °C ($[\text{G}_5\text{F-PA}] = [\text{G}_5\text{W-PA}] = 63 \mu\text{M}$, in HEPES saline buffer).

Self-assembled hydrogels based on PA-CB[8] host-guest interactions

CB[8] triggers PA hydrogelation

Having assessed how the formation of homoternary $(PA)_2 \subset CB[8]$ complexes occur at diluted concentration regimes, we then investigated whether this non-covalent union can be used to dynamically cross-link PA nanofibers at higher concentrations relevant to hydrogel formulation. When a 350 μ M solution of **CB[8]** was injected into a 6 mM **G₅F-PA** solution, a transparent 1 wt% gel was obtained. **G₅W-PA** rendered a more turbid gel, which has been associated to phase separation and aggregation of PA molecules.⁵⁵ Gelation of both PA solutions represented a macroscopic reflection of changes in self-assembly at the molecular level, therefore we proceeded to assess those changes in the microstructure of the hydrogels. Scanning electron microscopy (SEM) images revealed the presence of a 3D network comprising high aspect-ratio nanofibers similar to classical PA hydrogels when using **G₅F-PA/CB[8]** (Figure 4A). **G₅W-PA/CB[8]** hydrogels also exhibited 3D networks but comprising shorter fiber arrays (Figure 4E).

Thermally treated guest-PA solutions were also subjected to gelation via **CB[8]** complex formation. As expected, heat treated **G₅F-PA/CB[8]** hydrogels exhibited nanofiber alignment at the micro scale (Figure 4C), while thermally treated **G₅W-PA/CB[8]** hydrogels presented twisted filaments made of bundled peptide fibrils (Figure 4G, Figure S7). These results suggest that thermal treatment and interaction with **CB[8]** may promote parallel alignment of nanofibers into larger **G₅W-PA** constructs than non-gelated (Figure 1D) or non-heated ones (Figure 4E).

Similar bundled and twisted fiber morphologies of varying diameters have been reported by Stupp and co-workers^{56,28} who attributed this phenomena to large-scale spatial redistribution of molecules directed by either noncovalent electrostatics and Watson-Crick DNA base-pairing, and by exchange dynamics which create domains with highly concentrated host-guest interactions, respectively. Our

findings suggest that the combination of simple thermal treatment of nanofibrillar materials and the dynamic cross-linking ability of **CB[8]** can also lead to hierarchical ordering.

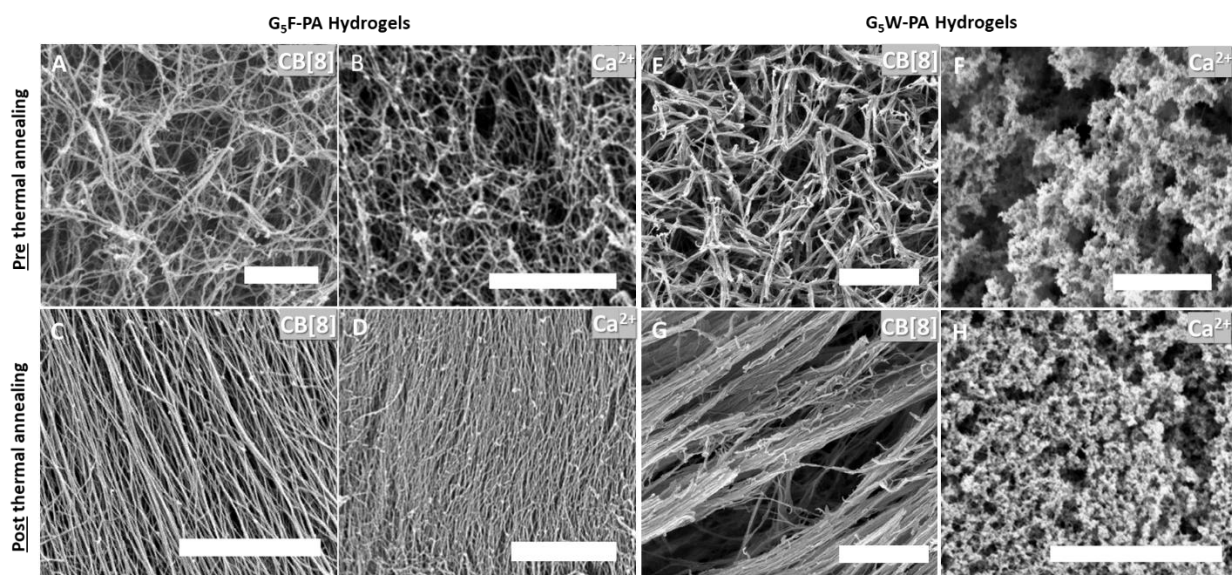


Figure 4. Microstructure analysis of PA-based hydrogels showing nanofiber persistence and alignment due to thermal treatment in **CB[8]** and Ca^{2+} -based hydrogels. A-D) SEM micrographs of **G₅F-PA** hydrogels: A) non-heated **CB[8]**-based B) non-heated Ca^{2+} -based C) heated **CB[8]**-based, and D) heated Ca^{2+} -based. E-H) SEM micrographs of **G₅W-PA** hydrogels: E) non-heated **CB[8]**-based F) non-heated Ca^{2+} -based G) heated **CB[8]**-based, and H) heated Ca^{2+} -based (1 wt% gels in all cases, [**CB[8]**] = 350 μM , [Ca^{2+}] = 50 mM, scale bars = 2 μm).

***CB[8]**-based versus Ca^{2+} -based PA hydrogelation*

When dissolved in water or aqueous media, PAs form viscous solutions which traditionally generate self-supporting hydrogels from solutions upon pH changes or addition of ionic species.⁵⁷ **G₅F-PA** and **G₅W-PA** were found to be no exception, as addition of CaCl_2 (as source of Ca^{2+} ions) rendered transparent hydrogels in every case. Room temperature **G₅F-PA** solutions generated anisotropic fibrillar 3D networks (Figure 4B) while thermally treated **G₅F-PA** solutions rendered aligned nanofibers (Figure 4D) similar to their analogue **CB[8]**-based hydrogels in both cases. **G₅W-PA** Ca^{2+} -based hydrogels exhibited significant morphological differences both in room temperature (Figure 4F) and thermally treated scenarios when compared to their **CB[8]**-based analogue hydrogels. No

fibrillar network formation was observed for **G₅W-PA** Ca²⁺-based hydrogels, only the presence of a continuous assembly of amorphous particles was found instead (Figure 4H).

In summary, both the host-guest-based mechanism and the traditional ion-based gelation approach rendered fiber formation and alignment in **G₅F-PA** hydrogels. However, the host-guest gelation mechanism allowed further structuring of aligned fibrillar morphologies in **G₅W-PA** hydrogels that the ion-bridging mechanism did not. These results also suggest that **CB[8]**-induced non-covalent crosslinking could be employed as a method to promote organization in non-covalent polymer-based biomaterials.

Mechanical properties of Guest PA-CB[8] hydrogels

Rheological characterisation of CB[8]-based PA hydrogels

Given these results, we reasoned that morphological differences in peptide architecture observed in **CB[8]**-based and Ca²⁺-based hydrogels should have impactful repercussions on the mechanical properties of the resulting materials. In order to test this hypothesis, hydrogel stiffness and response to deformation were assessed through oscillating rheology. Amplitude and frequency sweep experiments were used to quantify the storage modulus (G') and loss modulus (G'') of **CB[8]**-based hydrogels (Figure S8—S9). Viscoelastic behaviour was found in both thermally treated hydrogel systems, G' values were greater than G'' in every case, confirming that materials exhibit a predominantly elastic rather than viscous character (Figure 5).

G₅F-PA/CB[8] hydrogels exhibited significantly higher G' values (4.7 ± 1.3 kPa, $p < 0.0001$) than those of **G₅W-PA/CB[8]** hydrogels (1.2 ± 0.2 kPa, Figure 5C, Table S2). These differences can be attributed to the length of aligned fiber aggregates found in **G₅F-PA/CB[8]** (Figure 4C) compared to the shorter fibers and random aggregates found in **G₅W-PA/CB[8]** gels (Figure 4G, Figure S7). These findings are in agreement with reports on hydrogels comprising pendant phenylalanine or tryptophan amino acids, where the phenylalanine unit affords much stronger hydrogel materials than its tryptophan counterpart.⁴²

Stiffness of ion-based PA hydrogels can be tuned as a function of Ca^{2+} ions. We took advantage of this property to prepare **G₅F-PA** and **G₅W-PA** hydrogels with similar stiffness values to our dynamically crosslinked PA/**CB[8]** gels. **G₅F-PA**/ Ca^{2+} hydrogels required the use of $[\text{CaCl}_2] = 30$ mM to emulate stiffness values of **G₅F-PA**/**CB[8]** (crosslinked with $[\text{CB[8]}] = 350 \mu\text{M}$), whereas a higher CaCl_2 concentration of 50 mM was necessary in the case of **G₅W-PA**/ Ca^{2+} hydrogels prepared under equivalent conditions (Figure 5).

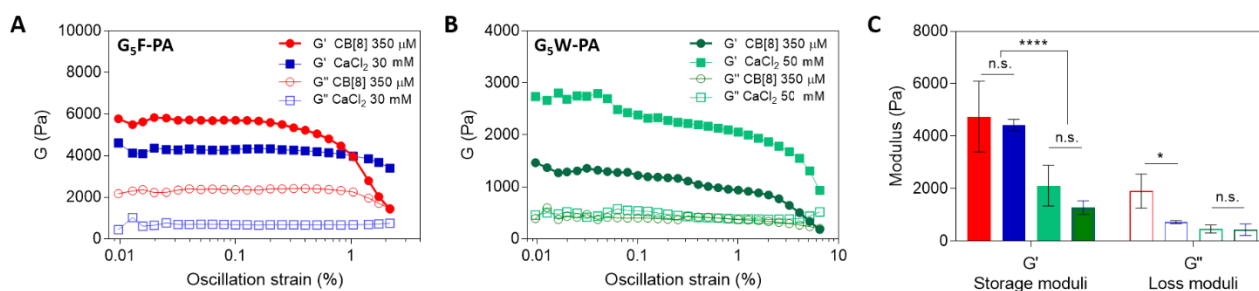


Figure 5. Dynamic rheology characterisation of **CB[8]**- and Ca^{2+} -based self-assembled hydrogels. A) Oscillation strain sweep experiments on 1 wt% **G₅F-PA** hydrogels based on **CB[8]** and Ca^{2+} ($[\text{CB[8]}] = 350 \mu\text{M}$, $[\text{CaCl}_2] = 30$ mM, from thermally treated PA solutions). B) Oscillation strain sweep experiments on 1 wt% **G₅W-PA** hydrogels based on **CB[8]** and CaCl_2 ($[\text{CB[8]}] = 350 \mu\text{M}$, $[\text{CaCl}_2] = 50$ mM, from thermally treated PA solutions). C) Storage (G') and loss (G'') moduli corresponding to **G₅F-PA** and **G₅W-PA** hydrogels (* $p < 0.05$, **** $p < 0.0001$, $n > 3$; n.s. no significant difference).

*Interfiber dynamics in **CB[8]**-based and Ca^{2+} -based hydrogels*

In Ca^{2+} -based hydrogels, self-assembly of PAs is triggered by electrostatic counterion screening while self-assembly of **CB[8]**-based hydrogels occurs due to hampering of aromatic amino acids mostly due to π - π interactions. Simple stoichiometry calculations show that formation of **CB[8]**-based hydrogels involved the presence of only one **CB[8]** molecule per every 30 aromatic binding sites in the guest-PA nanofibers periphery. However, in Ca^{2+} -based hydrogels, it took a 3:1 excess ratio of calcium ions to carboxylate binding sites to afford similar mechanical properties. The fact that the **CB[8]**-mediated gelation mechanism involves interfiber host-guest complexations among surface-located residues, while Ca^{2+} -mediated gelation requires cations to diffuse to the fiber core to shield

glutamic acid residues (which might be significantly shielded by the glycine linker and hydrophobic residue presented at the fiber surface) might play a role to explain these differences. It is known that additional interfiber interactions such as van der Waals and hydrophobic forces and hydrogen bonding take place during PA self-assembly.⁵⁷ Overall, our results indicate that host-guest interactions can drive more efficient PA gelation than electrostatic forces as the ones involved in Ca⁺²-based hydrogels.

Furthermore, rheological comparison of Ca⁺²-based and **CB[8]**-based hydrogels also revealed significant differences with respect to the loss tangent values. Loss tangent is a measure of the ratio of energy lost to energy stored during gel cyclic deformation,⁵⁸ and it can be easily calculated as $\tan \delta = G''/G'$. Our results confirmed that values of $\tan \delta$ for **G5F-PA** and **G5W-PA** Ca⁺²-based hydrogels were lower than those corresponding to equivalent **CB[8]**-based hydrogels, which indicates that the electrostatic mechanism of assembly generates hydrogels with greater elastic character than host-guest driven ones.

Even though both hydrogel classes rely on non-covalent interfiber contacts, transient and non-specific electrostatic ion bridging lack the intricacies of molecular binding and recognition events that lead to **CB[8]**-guest complex formation. The recruitment of a second interfiber PA monomer unit in our (Guest-PA)₂⊂**CB[8]** crosslinks ultimately determines the mechanical properties of the hydrogels. As supramolecular hydrogels translate molecular-scale information into material properties,⁵⁹ it is possible that interfiber fixation of PA anchoring points can limit sliding of the nanofibers during stress deformations. Evidences from the literature suggest that the residence time of guest molecules within an assembly and the entry and exit mechanism may determine the functionality of host units.⁶⁰ It has been reported that in **CB[8]**-phenylalanine and tryptophan covalent polymer-based systems the binding of the second aromatic guest dictates hydrogel stiffness, *i.e.* greater mechanical strength is produced as a result of higher energetic barrier of dissociation of the complex, which reflects in the residence time of guest moieties as part of the ternary complex which is the millisecond timescale.⁶¹

Reduction in PA dynamic exchange due to recruiting into binding sites has been observed in coarse-grained molecular dynamics simulations,⁵⁶ as well as in anionic host-guest PA-based hydrogels, where exchange among the molecules allowed the formation of supramolecular structures that concentrate host-guest interactions within the regions containing the bundled fibers of the superstructure.²⁸

Although both adamantane/ β -cyclodextrin and **CB[8]**-PA represent elegant host-guest interfiber crosslinking strategies, gelation via **CB[8]** involves a 2:1 stoichiometry, a higher affinity constant between PA monomers, improved elastic character, and yet a far less challenging synthetic approach for the preparation of host-PA molecules. These results show that **CB[8]**-PA complexations can be employed to modulate nanofiber morphology and mechanical performance of peptide fibers and their resulting hydrogels.

Biocompatibility of Guest PA-CB[8] hydrogels

Biological relevance of CB[8]-PA hydrogels

In general, PA-based hydrogels are suitable matrixes for cell culture as they can recapitulate mechanical and morphological features of the native ECM. PA-based hydrogels are known to be thixotropic. For example, ion-based PA hydrogels are known to exhibit shear-thinning and fast recovery properties⁶² and this thixotropic behaviour has also been reported by us for adamantane/ β -cyclodextrin host-guest PA hydrogels.²⁶ The Stupp Laboratory has exploited these properties for their use as inks for 3D bioprinting.²⁸ **CB[8]**-based PA hydrogels are also expected to exhibit these properties which are advantageous for both *in vitro* and *in vivo* applications involving fast-recovery administration routes. For example, *in vitro*, these matrixes can provide ECM-like environments for the study of calcium-sensitive cells, such as neurons⁶³ and mesenchymal stem cells.⁶⁴

Cell culture studies

To assess the applicability of the host-guest crosslinked PA hydrogels, *in vitro* culture of NIH-3T3 fibroblasts over **G₅F-PA** and **G₅W-PA** (both **CB[8]** and CaCl₂-based) hydrogels was performed. Both host-guest crosslinked and ion-based hydrogels exhibited similar cell viability values of over 95% after 24 h of culture compared to tissue culture plastic controls (Figure 6A, B). These results correlate with those obtained in cell viability assays in solution, as the presence of **CB[8]** proved not to be detrimental in the fibroblasts cell response, neither in the gel state nor when presented to a monolayer of cells in solution state (Figure S10). This result is relevant because one advantage of PA-based hydrogel platforms is the possibility to embed cells during the gelation process. In this scenario, cells will be in the presence of PA molecules in solution and, consequently, their viability is critical in these conditions.

Both herein explored gelation modes (calcium-based and **CB[8]**-based) rely on substantially different mechanisms, the former involving inner sections of self-assembled nanofibers and the latter connecting surface located guest-residues in PA monomers. Exploiting hydrogels involving both approaches for gel formation is an interesting possibility. Preliminary experiments with hydrogels obtained by simultaneous Ca²⁺ and **CB[8]**-driven gelation did not show differences in transparency compared to only Ca²⁺ and **CB[8]**-based hydrogels (Supporting Information, Section VIII). Nonetheless, thorough rheological characterization of such systems remains pending and requires further systematic studies. This synergistic use of both mechanisms could be exploited in circumstances where ion-rich environments or a precise gel architecture or stiffness are desired. Such systems could be used as disease models in calcification involved pathologies like heterotopic ossification (the formation of bone in soft tissues), where muscle or spinal cord injury animal models are used.⁶⁵

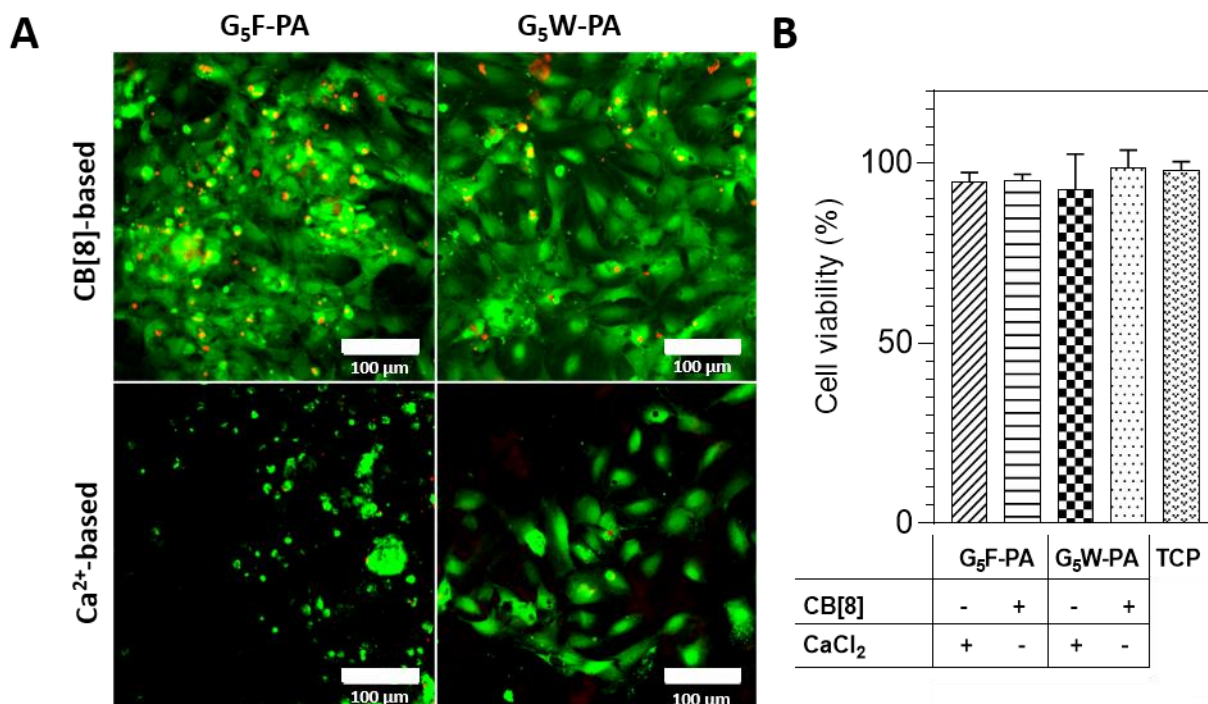


Figure 6. Cell viability studies of NIH-3T3 fibroblasts cultured onto **CB[8]** and Ca²⁺-based PA-hydrogels. A) LIVE/DEAD images from the cell-seeded hydrogels (green: calcein AM, alive cells; red: ethidium homodimer-1 (EthD-1), dead cells; scale bars = 100 μ m). B) Cell viability values after 24 h of culture onto **G₅F-PA** and **G₅W-PA** hydrogels ($[\text{CB}[8]] = 350 \mu\text{M}$, $[\text{CaCl}_2]_{\text{G5F}} = 30 \text{ mM}$, $[\text{CaCl}_2]_{\text{G5W}} = 50 \text{ mM}$, from thermally treated PA solutions, TCP = tissue culture plastic).

PA-based material platforms offer exciting opportunities to design a broad range of functional matrixes. **CB[8]**-crosslinked PA hydrogels are expected to exhibit increased stability, as they are not expected to be greatly affected by pH or by the presence of calcium-chelating agents. Modularity of **CB[8]**-based PA hydrogels offers the possibility to continuously vary the content of host-PA by using a filler-PA bearing neither glycine spacers nor aromatic residues, while also their ion-independent gelation mechanism might be relevant for *in vivo* scenarios where an excess of gelling counterions could become detrimental. For instance, ion-rich environments could influence enzyme activity and protein conformation, cause osmotic unbalances, hinder cargo delivery by formation of electrostatic complexes with drugs, or affect cell and organelle function.⁶⁶

Self-assembled systems like guest-PA/**CB[8]** offer the advantage of tunability as their modular preparation allows variation of the ratio of host-guest content. Future studies in this direction may explore the tuning of mechanical properties and porosity by adjusting the content and presentation mode of guest-PAs by using a diluent-filler PA to co-assemble with, in order to change the host:guest ratio without modification of the overall PA-content in the hydrogels.²⁸ Another crucial aspect that remains less exploited in host-guest-based PA hydrogels is the effect of temperature, as dynamic supramolecular complexations of such nature are known to be temperature-dependent. This temperature-dependent effect is expected to affect the hydrogels mechanical properties which should be investigated under more physiologically relevant conditions to promote the implementation of these hydrogels in *in vivo* applications.

It is an essential goal to strive for mimicking the dynamic spatiotemporal properties of the native ECM.^{14,67} A practical strategy to achieve this goal is the use dynamic non-covalent interactions. We believe that host-guest mediated PA hydrogels offer a practical toolkit to design such matrixes and we expect that further research on these systems can lead to hydrogel materials with a spectrum of dynamic, yet controllable, properties.

CONCLUSIONS

In this study, we report on the synthesis, supramolecular aggregation, and structural characterisation of the unreported **CB[8]**-guest mediated dimerization of PA nanofibers containing phenylalanine and tryptophan motifs. **CB[8]**-driven PA gelation and maintained PA nanofiber hierarchical organisation, represents a promising mechanism to understand and guide precision organisation and functionality in other supramolecular polymer-based biomaterials. The **CB[8]**-based hydrogels achieved similar mechanical properties and suitability for cell culture compared to hydrogels involving ion-rich conditions, while involving only a minimal fraction of interfiber contacts. Overall, our work evidences the benefits of merging the self-assembling dynamic properties of PA nanofibers with the

high stability of (Guest-PA)₂⊂**CB[8]** crosslinks. **CB[8]**-based PA hydrogels may find applications in the development of therapies for disease and regenerative medicine.

ASSOCIATED CONTENT

Supporting Information

Peptide amphiphile (PA) synthesis, purification, and characterisation. ¹H-NMR spectroscopy data, fluorescence spectroscopy spectra, scanning electron micrographs, dynamic rheology measurements, and cell viability assays on PA solutions.

AUTHOR INFORMATION

Corresponding authors

Alvaro Mata - School of Engineering & Materials Science, Queen Mary University of London, London E1 4NS, UK; Institute of Bioengineering, Queen Mary University of London, London E1 4NS, UK; School of Pharmacy, University of Nottingham, University Park, Nottingham NG7 2RD, UK; Department of Chemical and Environmental Engineering, University of Nottingham, University Park, Nottingham NG7 2RD, UK; Biodiscovery Institute, University of Nottingham, University Park, NG7 2RD, UK; Email: a.mata@nottingham.ac.uk

Helena S. Azevedo - School of Engineering & Materials Science, Queen Mary University of London, London E1 4NS, UK; Institute of Bioengineering, Queen Mary University of London, London E1 4NS, UK; Email: h.azevedo@qmul.ac.uk

Authors

Carlos Redondo-Gómez - School of Engineering & Materials Science, Queen Mary University of London, London E1 4NS, UK; Institute of Bioengineering, Queen Mary University of London, London E1 4NS, UK; National Nanotechnology Laboratory LANOTEC, National Center for High Technology CeNAT, 1174-1200 Pavas, San José, Costa Rica.

Soraya Padilla-Lopátegui - School of Engineering & Materials Science, Queen Mary University of London, London E1 4NS, UK; Institute of Bioengineering, Queen Mary University of London, London E1 4NS, UK.

AUTHOR CONTRIBUTIONS

The manuscript was written through contributions of all authors. All authors have given approval to the final version of the manuscript.

NOTES

There are no conflicts to declare.

ACKNOWLEDGEMENTS

This work was financially supported by the European Research Council (ERC) Starting Grant (STROFUNSCAFF), the Medical Research Council (UK Regenerative Medicine Platform Acellular/Smart Materials-3D Architecture, MR/R015651/1), and the Program for Innovation and Human Capital from the Ministry of Science, Technology and Telecommunications of the Government of Costa Rica (MICITT-PINN-PED-014-2015-2). The authors thank everyone in the Mata and Azevedo Groups for valuable discussions.

REFERENCES

- (1) Lehn, J. M. Toward Self-Organization and Complex Matter. *Science* (80-.). **2002**, 295 (5564), 2400–2403. <https://doi.org/10.1126/science.1071063>.
- (2) Mendes, A. C.; Baran, E. T.; Reis, R. L.; Azevedo, H. S. Self-Assembly in Nature: Using the Principles of Nature to Create Complex Nanobiomaterials. *Wiley Interdiscip. Rev. Nanomedicine Nanobiotechnology* **2013**, 5 (6), 582–612. <https://doi.org/10.1002/wnan.1238>.
- (3) Lutz, J.-F.; Lehn, J.-M.; Meijer, E. W.; Matyjaszewski, K. From Precision Polymers to

Complex Materials and Systems. *Nat. Rev. Mater.* **2016**, *1* (5), 16024.

<https://doi.org/10.1038/natrevmats.2016.24>.

- (4) Radvar, E.; Azevedo, H. S. Supramolecular Peptide/Polymer Hybrid Hydrogels for Biomedical Applications. *Macromol. Biosci.* **2019**, *19* (1), 1–16.
<https://doi.org/10.1002/mabi.201800221>.
- (5) Paolino, M.; Ennen, F.; Lamponi, S.; Cernescu, M.; Voit, B.; Cappelli, A.; Appelhans, D.; Komber, H. Cyclodextrin-Adamantane Host–Guest Interactions on the Surface of Biocompatible Adamantyl-Modified Glycodendrimers. *Macromolecules* **2013**, *46* (9), 3215–3227. <https://doi.org/10.1021/ma400352m>.
- (6) Gačanin, J.; Synatschke, C. V.; Weil, T. Biomedical Applications of DNA-Based Hydrogels. *Adv. Funct. Mater.* **2019**, *1906253*. <https://doi.org/10.1002/adfm.201906253>.
- (7) Luo, Q.; Hou, C.; Bai, Y.; Wang, R.; Liu, J. Protein Assembly: Versatile Approaches to Construct Highly Ordered Nanostructures. *Chem. Rev.* **2016**, *116* (22), 13571–13632.
<https://doi.org/10.1021/acs.chemrev.6b00228>.
- (8) Ulijn, R. V.; Lampel, A. Order/Disorder in Protein and Peptide-Based Biomaterials. *Isr. J. Chem.* **2019**, 1–13. <https://doi.org/10.1002/ijch.201900051>.
- (9) Dasgupta, A.; Mondal, J. H.; Das, D. Peptide Hydrogels. *RSC Adv.* **2013**, *3* (24), 9117–9149.
<https://doi.org/10.1039/c3ra40234g>.
- (10) Ulijn, R. V.; Smith, A. M. Designing Peptide Based Nanomaterials. *Chem. Soc. Rev.* **2008**, *37* (4), 664–675. <https://doi.org/10.1039/b609047h>.
- (11) Okesola, B. O.; Mata, A. Multicomponent Self-Assembly as a Tool to Harness New Properties from Peptides and Proteins in Material Design. *Chem. Soc. Rev.* **2018**, *47* (10), 3721–3736. <https://doi.org/10.1039/c8cs00121a>.

- (12) Dou, X. Q.; Feng, C. L. Amino Acids and Peptide-Based Supramolecular Hydrogels for Three-Dimensional Cell Culture. *Adv. Mater.* **2017**, *29* (16), 1–21.
<https://doi.org/10.1002/adma.201604062>.
- (13) Hartgerink, J. D.; Beniash, E.; Stupp, S. I. Self-Assembly and Mineralization of Peptide-Amphiphile Nanofibers. *Science (80-.)*. **2001**, *294* (5547), 1684–1688.
<https://doi.org/10.1126/science.1063187>.
- (14) Hussey, G. S.; Dziki, J. L.; Badylak, S. F. Extracellular Matrix-Based Materials for Regenerative Medicine. *Nat. Rev. Mater.* **2018**, *3* (7), 159–173.
<https://doi.org/10.1038/s41578-018-0023-x>.
- (15) Zhang, S.; Greenfield, M. A.; Mata, A.; Palmer, L. C.; Bitton, R.; Mantei, J. R.; Aparicio, C.; de la Cruz, M. O.; Stupp, S. I. A Self-Assembly Pathway to Aligned Monodomain Gels. *Nat. Mater.* **2010**, *9* (7), 594–601. <https://doi.org/10.1038/nmat2778>.
- (16) Silva, G. A.; Silva, G. A.; Czeisler, C.; Niece, K. L.; Beniash, E.; Harrington, D. A.; Kessler, J. A.; Stupp, S. I. Selective Differentiation of Neural Progenitor Cells by High – Epitope Density Nanofibers. *Science (80-.)*. **2014**, *303* (February), 1352–1355.
<https://doi.org/10.1126/science.1093783>.
- (17) McClendon, M. T.; Yalom, A.; Berns, E. J.; Hokugo, A.; Stupp, S. I.; Jarrahy, R.; Spigelman, I.; Li, A.; Stephanopoulos, N.; Segovia, L. A. A Bioengineered Peripheral Nerve Construct Using Aligned Peptide Amphiphile Nanofibers. *Biomaterials* **2014**, *35* (31), 8780–8790.
<https://doi.org/10.1016/j.biomaterials.2014.06.049>.
- (18) Webber, M. J.; Tongers, J.; Newcomb, C. J.; Marquardt, K.-T.; Bauersachs, J.; Losordo, D. W.; Stupp, S. I. Supramolecular Nanostructures That Mimic VEGF as a Strategy for Ischemic Tissue Repair. *Proc. Natl. Acad. Sci.* **2011**, *108* (33), 13438–13443.
<https://doi.org/10.1073/pnas.1016546108>.

- (19) Mata, A.; Geng, Y.; Henrikson, K. J.; Aparicio, C.; Stock, S. R.; Satcher, R. L.; Stupp, S. I. Bone Regeneration Mediated by Biomimetic Mineralization of a Nanofiber Matrix. *Biomaterials* **2010**, *31* (23), 6004–6012. <https://doi.org/10.1016/j.biomaterials.2010.04.013>.
- (20) Shah, R. N.; Shah, N. A.; Del Rosario Lim, M. M.; Hsieh, C.; Nuber, G.; Stupp, S. I. Supramolecular Design of Self-Assembling Nanofibers for Cartilage Regeneration. *Proc. Natl. Acad. Sci.* **2010**, *107* (8), 3293–3298. <https://doi.org/10.1073/pnas.0906501107>.
- (21) Derkus, B.; Okesola, B. O.; Barrett, D. W.; D'Este, M.; Chowdhury, T. T.; Eglin, D.; Mata, A. Multicomponent Hydrogels for the Formation of Vascularized Bone-like Constructs in Vitro. *Acta Biomater.* **2020**, *109*, 82–94. <https://doi.org/10.1016/j.actbio.2020.03.025>.
- (22) Hedegaard, C. L.; Redondo-Gómez, C.; Tan, B. Y.; Ng, K. W.; Loessner, D.; Mata, A. Peptide-Protein Coassembling Matrices as a Biomimetic 3D Model of Ovarian Cancer. *Sci. Adv.* **2020**, *6* (40). <https://doi.org/10.1126/sciadv.abb3298>.
- (23) Mantooth, S. M.; Munoz-Robles, B. G.; Webber, M. J. Dynamic Hydrogels from Host–Guest Supramolecular Interactions. *Macromol. Biosci.* **2019**, *19* (1), 1–12. <https://doi.org/10.1002/mabi.201800281>.
- (24) Vázquez-González, M.; Willner, I. Stimuli-Responsive Biomolecule-Based Hydrogels and Their Applications. *Angew. Chemie Int. Ed.* **2019**, [10.1002/anie.201907670](https://doi.org/10.1002/anie.201907670). <https://doi.org/10.1002/anie.201907670>.
- (25) Rosales, A. M.; Anseth, K. S. The Design of Reversible Hydrogels to Capture Extracellular Matrix Dynamics. *Nat. Rev. Mater.* **2016**, *1* (2), 1–15. <https://doi.org/10.1038/natrevmats.2015.12>.
- (26) Redondo-Gómez, C.; Abdouni, Y.; Becer, C. R.; Mata, A. Self-Assembling Hydrogels Based on a Complementary Host–Guest Peptide Amphiphile Pair. *Biomacromolecules* **2019**, *20* (6), 2276–2285. <https://doi.org/10.1021/acs.biomac.9b00224>.

- (27) Redondo-Gómez, C.; Padilla-Lopategui, S.; Azevedo, H. S.; Mata, A. Host–Guest-Mediated Epitope Presentation on Self-Assembled Peptide Amphiphile Hydrogels. *ACS Biomater. Sci. Eng.* **2020**, *6* (9), 4870–4880. <https://doi.org/10.1021/acsbiomaterials.0c00549>.
- (28) Edelbrock, A. N.; Clemons, T. D.; Chin, S. M.; Roan, J. J. W.; Bruckner, E. P.; Álvarez, Z.; Edelbrock, J. F.; Wek, K. S.; Stupp, S. I. Superstructured Biomaterials Formed by Exchange Dynamics and Host–Guest Interactions in Supramolecular Polymers. *Adv. Sci.* **2021**, *8* (8), 2004042. <https://doi.org/10.1002/advs.202004042>.
- (29) Lagona, J.; Mukhopadhyay, P.; Chakrabarti, S.; Isaacs, L. The Cucurbit[n]Urils Family. *Angew. Chemie - Int. Ed.* **2005**, *44* (31), 4844–4870. <https://doi.org/10.1002/anie.200460675>.
- (30) Das, D.; Scherman, O. A. Cucurbituril: At the Interface of Small Molecule Host-Guest Chemistry and Dynamic Aggregates. *Isr. J. Chem.* **2011**, *51* (5–6), 537–550. <https://doi.org/10.1002/ijch.201100045>.
- (31) Appel, E. A.; Del Barrio, J.; Loh, X. J.; Scherman, O. A. Supramolecular Polymeric Hydrogels. *Chem. Soc. Rev.* **2012**, *41* (18), 6195–6214. <https://doi.org/10.1039/c2cs35264h>.
- (32) Barrow, S. J.; Kasera, S.; Rowland, M. J.; Del Barrio, J.; Scherman, O. A. Cucurbituril-Based Molecular Recognition. *Chem. Rev.* **2015**, *115* (22), 12320–12406. <https://doi.org/10.1021/acs.chemrev.5b00341>.
- (33) Pazos, E.; Novo, P.; Peinador, C.; Kaifer, A. E.; García, M. D. Cucurbit[8]Urils (CB[8])-Based Supramolecular Switches. *Angew. Chemie - Int. Ed.* **2019**, *58* (2), 403–416. <https://doi.org/10.1002/anie.201806575>.
- (34) Wu, G.; Clarke, D. E.; Wu, C.; Scherman, O. A. Oligopeptide-CB[8] Complexation with Switchable Binding Pathways. *Org. Biomol. Chem.* **2019**, *17* (14), 3514–3520. <https://doi.org/10.1039/c9ob00592g>.
- (35) Heitmann, L. M.; Taylor, A. B.; Hart, P. J.; Urbach, A. R. Sequence-Specific Recognition

and Cooperative Dimerization of N-Terminal Aromatic Peptides in Aqueous Solution by a Synthetic Host. *J. Am. Chem. Soc.* **2006**, *128* (38), 12574–12581.

<https://doi.org/10.1021/ja064323s>.

- (36) Sonzini, S.; Ryan, S. T. J.; Scherman, O. A. Supramolecular Dimerisation of Middle-Chain Phe Pentapeptides via CB[8] Host-Guest Homoternary Complex Formation. *Chem. Commun.* **2013**, *49* (78), 8779–8781. <https://doi.org/10.1039/c3cc45420g>.
- (37) Zhao, L.; Xu, J.; Dong, Z.; Luo, Q.; Liu, J.; Li, J.; Zhang, W.; Hou, C. Construction of Protein Nanowires through Cucurbit[8]Uril-Based Highly Specific Host-Guest Interactions: An Approach to the Assembly of Functional Proteins. *Angew. Chemie Int. Ed.* **2013**, *52* (21), 5590–5593. <https://doi.org/10.1002/anie.201300692>.
- (38) Dang, D. T.; Nguyen, H. D.; Merckx, M.; Brunsveld, L. Supramolecular Control of Enzyme Activity through Cucurbit[8]Uril-Mediated Dimerization. *Angew. Chemie - Int. Ed.* **2013**, *52* (10), 2915–2919. <https://doi.org/10.1002/anie.201208239>.
- (39) Rowland, M. J.; Atgie, M.; Hoogland, D.; Scherman, O. A. Preparation and Supramolecular Recognition of Multivalent Peptide-Polysaccharide Conjugates by Cucurbit[8]Uril in Hydrogel Formation. *Biomacromolecules* **2015**, *16* (8), 2436–2443. <https://doi.org/10.1021/acs.biomac.5b00680>.
- (40) Qiao, H.; Jia, J.; Shen, H.; Zhao, S.; Chen, E.; Chen, W.; Di, B.; Hu, C. Capping Silica Nanoparticles with Tryptophan-Mediated Cucurbit[8]Uril Complex for Targeted Intracellular Drug Delivery Triggered by Tumor-Overexpressed IDO1 Enzyme. *Adv. Healthc. Mater.* **2019**, *8* (13). <https://doi.org/10.1002/adhm.201900174>.
- (41) Fenton, O. S.; Tibbitt, M. W.; Appel, E. A.; Jhunjhunwala, S.; Webber, M. J.; Langer, R. Injectable Polymer-Nanoparticle Hydrogels for Local Immune Cell Recruitment. *Biomacromolecules* **2019**, *20*, 4430–4436. <https://doi.org/10.1021/acs.biomac.9b01129>.

- (42) Rowland, M. J.; Appel, E. A.; Coulston, R. J.; Scherman, O. A. Dynamically Crosslinked Materials via Recognition of Amino Acids by Cucurbit[8]Urils. *J. Mater. Chem. B* **2013**, *1* (23), 2904. <https://doi.org/10.1039/c3tb20180e>.
- (43) Mata, A.; Palmer, L.; Tejada-Montes, E.; Stupp, S. I. Design of Biomolecules for Nanoengineered Biomaterials for Regenerative Medicine; Humana Press: Totowa, NJ, 2012; Vol. 811, pp 39–49. https://doi.org/10.1007/978-1-61779-388-2_3.
- (44) Sur, S.; Tantakitti, F.; Matson, J. B.; Stupp, S. I. Epitope Topography Controls Bioactivity in Supramolecular Nanofibers. *Biomater. Sci.* **2015**, *3* (3), 520–532. <https://doi.org/10.1039/c4bm00326h>.
- (45) Shi, Y.; Wareham, D. W.; Yuan, Y.; Deng, X.; Mata, A.; Azevedo, H. S. Polymyxin B-Triggered Assembly of Peptide Hydrogels for Localized and Sustained Release of Combined Antimicrobial Therapy. *Adv. Healthc. Mater.* **2021**, 2101465. <https://doi.org/10.1002/adhm.202101465>.
- (46) Shi, Y.; Ferreira, D. S.; Banerjee, J.; Pickford, A. R.; Azevedo, H. S. Tuning the Matrix Metalloproteinase-1 Degradability of Peptide Amphiphile Nanofibers through Supramolecular Engineering. *Biomater. Sci.* **2019**, *7* (12), 5132–5142. <https://doi.org/10.1039/C9BM00949C>.
- (47) Sleep, E.; Cosgrove, B. D.; McClendon, M. T.; Preslar, A. T.; Chen, C. H.; Sangji, M. H.; Pérez, C. M. R.; Haynes, R. D.; Meade, T. J.; Blau, H. M.; et al. Injectable Biomimetic Liquid Crystalline Scaffolds Enhance Muscle Stem Cell Transplantation. *Proc. Natl. Acad. Sci.* **2017**, *114* (38), E7919–E7928. <https://doi.org/10.1073/pnas.1708142114>.
- (48) Renny, J. S.; Tomasevich, L. L.; Tallmadge, E. H.; Collum, D. B. Method of Continuous Variations: Applications of Job Plots to the Study of Molecular Associations in Organometallic Chemistry. *Angew. Chemie - Int. Ed.* **2013**, *52* (46), 11998–12013.

<https://doi.org/10.1002/anie.201304157>.

- (49) Pashuck, E. T.; Cui, H.; Stupp, S. I. Tuning Supramolecular Rigidity of Peptide Fibers through Molecular Structure. *J. Am. Chem. Soc.* **2010**, *132* (17), 6041–6046.
<https://doi.org/10.1021/ja908560n>.
- (50) Freskgard, P. O.; Mårtensson, L. G.; Jonasson, P.; Jonsson, B. H.; Carlsson, U. Assignment of the Contribution of the Tryptophan Residues to the Circular Dichroism Spectrum of Human Carbonic Anhydrase II. *Biochemistry* **1994**, *33* (47), 14281–14288.
<https://doi.org/10.1021/bi00251a041>.
- (51) Andersson, D.; Carlsson, U.; Freskgard, P. O. Contribution of Tryptophan Residues to the CD Spectrum of the Extracellular Domain of Human Tissue Factor: Application in Folding Studies and Prediction of Secondary Structure. *Eur. J. Biochem.* **2001**, *268* (4), 1118–1128.
<https://doi.org/10.1046/j.1432-1327.2001.01981.x>.
- (52) Woody, R. W. Contributions of Tryptophan Side Chains to the Far-Ultraviolet Circular Dichroism of Proteins. *Eur. Biophys. J.* **1994**, *23* (4), 253–262.
<https://doi.org/10.1007/BF00213575>.
- (53) Diaferia, C.; Balasco, N.; Sibillano, T.; Giannini, C.; Vitagliano, L.; Morelli, G.; Accardo, A. Structural Characterization of Self-Assembled Tetra-Tryptophan Based Nanostructures: Variations on a Common Theme. *ChemPhysChem* **2018**, *19* (13), 1635–1642.
<https://doi.org/10.1002/cphc.201800026>.
- (54) Cosani, A.; Peggion, E.; Terbojevich, M.; Portolan, A. Optical Rotatory Dispersion of Poly-L-Tryptophan in the Far Ultraviolet Region. *Chem. Commun.* **1967**, No. 18, 930–931.
<https://doi.org/10.1039/C19670000930>.
- (55) Stendahl, J. C.; Rao, M. S.; Guler, M. O.; Stupp, S. I.; Stendahl, B. J. C.; Rao, M. S.; Guler, M. O.; Stupp, S. I. Intermolecular Forces in the Self-Assembly of Peptide Amphiphile

Nanofibers. *Adv. Funct. Mater.* **2006**, *16* (4), 499–508.

<https://doi.org/10.1002/adfm.200500161>.

- (56) Freeman, R.; Han, M.; Álvarez, Z.; Lewis, J. A.; Wester, J. R.; Stephanopoulos, N.; McClendon, M. T.; Lynsky, C.; Godbe, J. M.; Sangji, H.; et al. Reversible Self-Assembly of Superstructured Networks. *Science* (80-.). **2018**, *362* (6416), 808–813.
<https://doi.org/10.1126/science.aat6141>.
- (57) Stendahl, J. C.; Rao, M. S.; Guler, M. O.; Stupp, S. I. Intermolecular Forces in the Self-Assembly of Peptide Amphiphile Nanofibers. *Adv. Funct. Mater.* **2006**, *16* (4), 499–508.
<https://doi.org/10.1002/adfm.200500161>.
- (58) Murata, H. Rheology - Theory and Application to Biomaterials. In *Polymerization*; InTech, 2012; pp 403–423. <https://doi.org/10.5772/48393>.
- (59) Chivers, P. R. A.; Smith, D. K. Shaping and Structuring Supramolecular Gels. *Nat. Rev. Mater.* **2019**, *4* (7), 463–478. <https://doi.org/10.1038/s41578-019-0111-6>.
- (60) Davis, A. V.; Yeh, R. M.; Raymond, K. N. Supramolecular Assembly Dynamics. *Proc. Natl. Acad. Sci.* **2002**, *99* (8), 4793–4796. <https://doi.org/10.1073/pnas.052018299>.
- (61) Appel, E. A.; Forster, R. A.; Koutsioubas, A.; Toprakcioglu, C.; Scherman, O. A. Activation Energies Control the Macroscopic Properties of Physically Cross-Linked Materials. *Angew. Chemie - Int. Ed.* **2014**, *53* (38), 10038–10043. <https://doi.org/10.1002/anie.201403192>.
- (62) Greenfield, M. A.; Hoffman, J. R.; De La Cruz, M. O.; Stupp, S. I. Tunable Mechanics of Peptide Nanofiber Gels. *Langmuir* **2010**, *26* (5), 3641–3647.
<https://doi.org/10.1021/la9030969>.
- (63) Berridge, M. J. Neuronal Calcium Signaling. *Neuron* **1998**, *21* (1), 13–26.
[https://doi.org/10.1016/S0896-6273\(00\)80510-3](https://doi.org/10.1016/S0896-6273(00)80510-3).

- (64) Lee, M. N.; Hwang, H.-S.; Oh, S.-H.; Roshanzadeh, A.; Kim, J.-W.; Song, J. H.; Kim, E.-S.; Koh, J.-T. Elevated Extracellular Calcium Ions Promote Proliferation and Migration of Mesenchymal Stem Cells via Increasing Osteopontin Expression. *Exp. Mol. Med.* **2018**, *50* (11), 1–16. <https://doi.org/10.1038/s12276-018-0170-6>.
- (65) Meyers, C.; Lisiecki, J.; Miller, S.; Levin, A.; Fayad, L.; Ding, C.; Sono, T.; McCarthy, E.; Levi, B.; James, A. W. Heterotopic Ossification: A Comprehensive Review. *JBMR Plus* **2019**, *3* (4), e10172. <https://doi.org/10.1002/jbm4.10172>.
- (66) Calvo-Rodriguez, M.; Hou, S. S.; Snyder, A. C.; Kharitonova, E. K.; Russ, A. N.; Das, S.; Fan, Z.; Muzikansky, A.; Garcia-Alloza, M.; Serrano-Pozo, A.; et al. Increased Mitochondrial Calcium Levels Associated with Neuronal Death in a Mouse Model of Alzheimer's Disease. *Nat. Commun.* **2020**, *11* (1), 2146. <https://doi.org/10.1038/s41467-020-16074-2>.
- (67) Rosales, A. M.; Vega, S. L.; DelRio, F. W.; Burdick, J. A.; Anseth, K. S. Hydrogels with Reversible Mechanics to Probe Dynamic Cell Microenvironments. *Angew. Chemie - Int. Ed.* **2017**, *56* (40), 12132–12136. <https://doi.org/10.1002/anie.201705684>.